Auditory Spatial Receptive Fields Created by Multiplication

José Luis Peña* and Masakazu Konishi

Examples of multiplication by neurons or neural circuits are scarce, although many computational models use this basic operation. The owl's auditory system computes interaural time (ITD) and level (ILD) differences to create a two-dimensional map of auditory space. Space-specific neurons are selective for combinations of ITD and ILD, which define, respectively, the horizontal and vertical dimensions of their receptive fields. A multiplication of separate postsynaptic potentials tuned to ITD and ILD, rather than an addition, can account for the subthreshold responses of these neurons to ITD-ILD pairs. Other nonlinear processes improve the spatial tuning of the spike output and reduce the fit to the multiplicative model.

Space-specific neurons in the owl's auditory map of space represent the results of all computations involved in the determination of the ITD and ILD that define the owl's auditory space (*1*, *2*). The parallel pathways that process these cues merge in the external nucleus of the inferior colliculus (ICx) to confer on the space-specific neurons selectivity for combinations of ITD and ILD (*3*, *4*) (Fig. 1A). How do postsynaptic potentials (psps) from the two sources interact to produce subthreshold and suprathreshold responses to ITD-ILD pairs?

Clusters of similar ITD-ILD pairs elicited suprathreshold depolarizing psps, whereas other ITD-ILD pairs induced hyperpolarization (Fig. 1C) (*5*–*8*). These response properties underlie the center excitatory and surround inhibitory organization of receptive fields (Fig. 1D) (*9*). All the neurons studied behaved like analog AND gates of ITD and ILD, suggesting that the two inputs are multiplied instead of being added. We used the method of singular value decomposition (svd) to show multiplication (*10*). This technique transforms a matrix into a weighted sum of the products of two independent vectors, called "singular vectors." The contribution of these products to the original matrix is ranked by the elements ("singular values") of a diagonal matrix.

The following example illustrates how the method works using the data obtained from a space-specific neuron. The responses of the neuron to ITD-ILD pairs were arranged in a matrix, M, in which ILD and ITD varied along rows and columns, respectively (Fig. 2A). We tested the hypothesis that the matrix contains constant and multiplicative components as in the following equation:

$$M(i,j) = V_o + \lambda U(i)V(j)^T \qquad (1)$$

where V_o represents a membrane potential offset. The second term indicates the multiplicative interaction between ITD and ILD inputs. $U(i)$ and $V(j)$ are the ITD and ILD inputs and λ is a singular value. The svd of M yielded nearly constant first singular vectors, confirming that the dominant term in M was an offset membrane voltage V_o (blue area in Fig. 2B). We determined the optimal V_o value in the equation ($V_o = -66.8$ mV in this example) by minimizing the sum of the squared singular values other than the first one in the svd of $M - V_o$. This procedure maximizes the difference in fractional energy or weight between the first and the remaining singular values of $M - V_o$ and is equivalent to a least squares fit to the multiplicative model. For all neurons, the best V_o was usually close to the maximal level of hyperpolarization, corresponding to the deepest trough of ITD curves. An svd of the sample matrix after V_o subtraction showed 98.57% of the energy in the first singular value and 0.96% in the second. Thus, a major part of the data matrix consists of a constant offset membrane voltage V_o and a multiplication product. Computation of U_1 and V_1 (first left and right singular vectors) of $M - V_o$ (Fig. 2, E and F) yielded functions similar to the neuron's measured ITD and ILD response

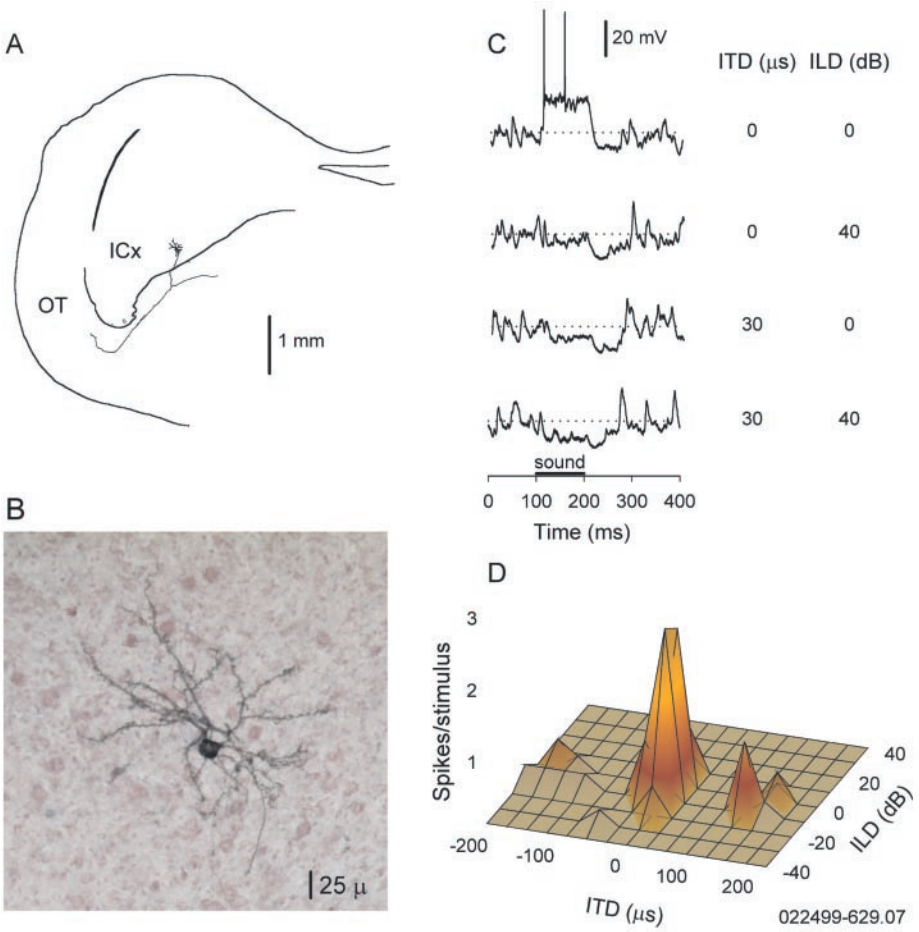

Fig. 1. Space-specific neuron. (**A**) A drawing of an ICx neuron and its axon projecting to the optic tectum (OT). (**B**) The same neuron labeled with neurobiotin. (**C**) Postsynaptic potentials in response to different ITD-ILD pairs. Dotted lines indicate the mean resting potential. (**D**) Spiking responses of the same neuron to different ITD-ILD pairs. The large peak is the excitatory center and the flat area around it is the inhibitory surround [compare (C) and (D)]. Negative (–)ITD and negative (–)ILD mean, respectively, sound in ipsilateral ear leading and louder.

Division of Biology 216-76, California Institute of Technology, Pasadena, CA 91125, USA.

*To whom correspondence should be addressed. E-mail jose@etho.caltech.edu

curves, once V_o was added (*11*) (Fig. 2, C and D). Finally, we verified that the equation provided a close approximation of the original matrix (Fig. 2B). This finding confirms that ITD and ILD inputs are independent of each other, as previously shown by other methods (*3*, *4*).

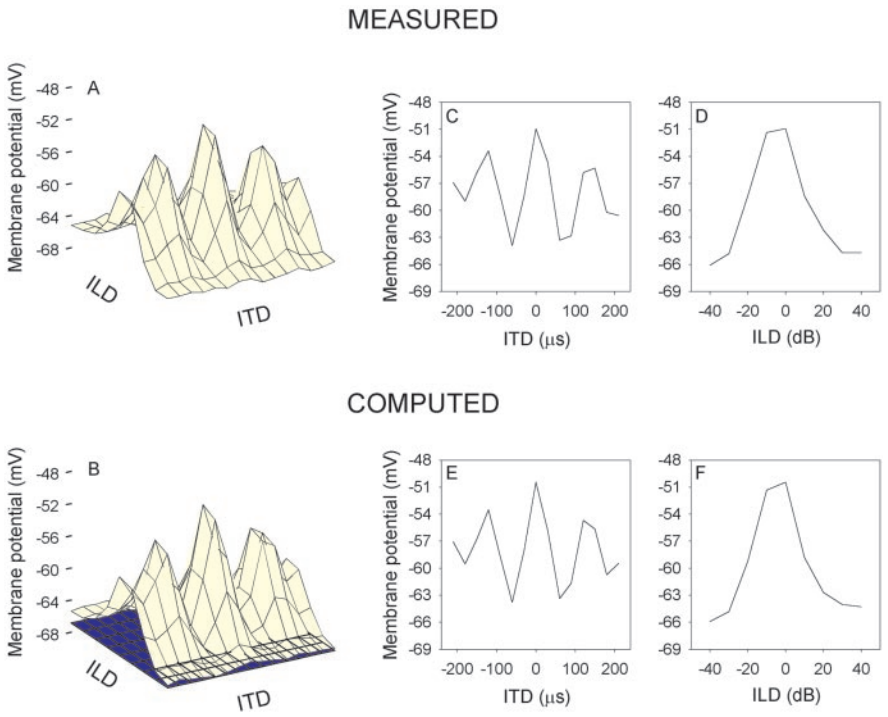

Fig. 2. Multiplicative combination of ILD and ITD inputs. (**A**) Raw data matrix. (**B**) Reconstruction of the matrix from the computed left and right singular vectors and the first singular value. Addition of V_o [DC offset (blue area)] that minimizes the second singular value almost restores the original matrix. (**C**) ITD curve. (**D**) ILD curve. (**E**) Computed left singular vector. (**F**) Computed right singular vector.

We tested the multiplicative hypothesis in 15 neurons in which we obtained responses for a large number of ITD-ILD pairs. All neurons showed similar trends to those described in the example mentioned above. After subtraction of V_o, the first singular value yielded a mean fractional energy of 96.6 ± 2.1% (Fig. 3A). We also examined which lower ranking singular values (second, third, etc.) were above the variability of the data and within the confidence interval of the first singular value. For a confidence level of 99.9% (*12*) with 4 degrees of freedom and the largest standard deviation, all singular values other than the first one were within the noise of our measurement in seven neurons. In these cases, 100% of the energy was in the first singular value. The first and second singular values were above the noise level in the remaining eight neurons (Fig. 3B). In these cases, the energy in the first singular value was 97.9 ± 0.9%. Thus, multiplication accounts for a large part of the observed responses in all neurons.

We also tested an additive model for comparison with the multiplicative model. A pure additive combination of ITD and ILD inputs can be given by

$$M(i,j) = V_m + F(i) + G(j) \qquad (2)$$

V_m is a constant and corresponds to the mean membrane potential. $F(i)$ and $G(j)$

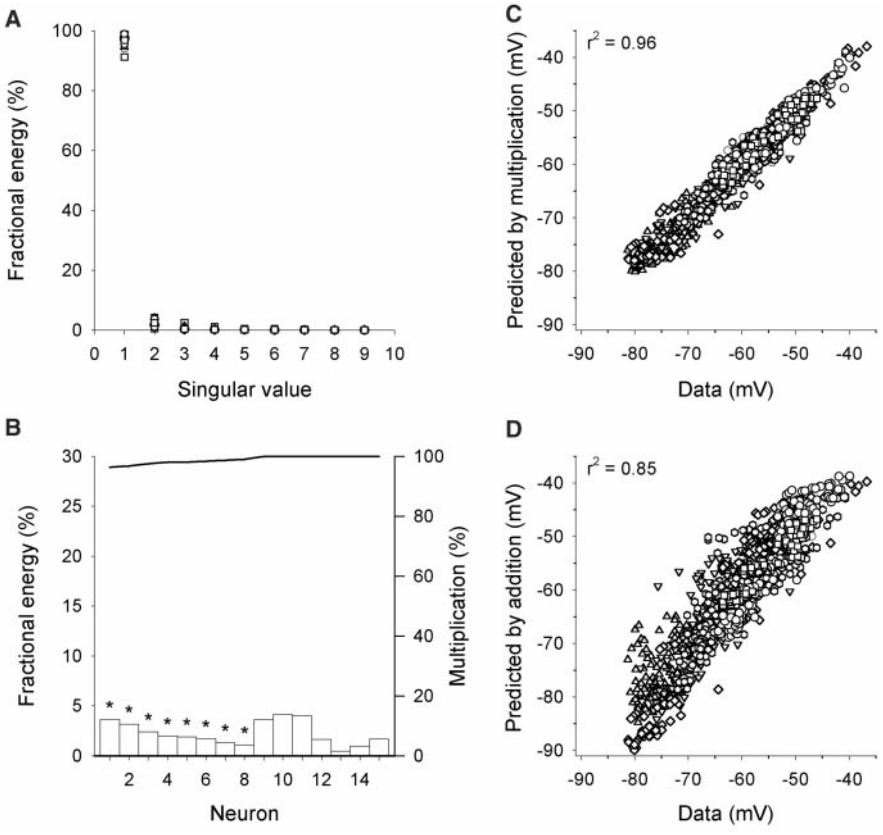

Fig. 3. Comparison of multiplicative and additive models for psps data. (**A**) Fractional energy of singular values for psps data in 15 neurons. A mean of 96.6 ± 2.1% of energy was in the first singular value in this sample of neurons. This plot appears sparse, because values from different neurons coincide extensively. (**B**) Fractional energy in the second singular values (bar graphs) after subtracting an offset. Asterisks indicate those cases in which the second singular value was above noise level. The solid line [multiplication (%) axis on the right] indicates the percent contribution of multiplicative processes when only the singular values above noise level are used in the computation of fractional energy. This value reaches 100% in those cases in which only the first singular value is larger than noise. (**C**) Correlation between the predicted response by multiplication and the original data for all the neurons. (**D**) Correlation is better with the multiplicative model than with the additive model.

represent the ITD and ILD inputs and were obtained by averaging rows and columns of $M - V_m$, respectively. However, this model could not reconstruct the original data matrix as well as the multiplicative model (Fig. 3, C and D). The error of the fit to the original data was significantly larger for the additive model than for the multiplicative one (F test, $P < 0.002$). We also considered the possibility of both multiplication and addition contributing to the subthreshold responses of space-specific neurons. However, a combination of addition and multiplication turned out to be nothing but multiplication. Therefore, the above comparison of the multiplicative and additive models should suffice to show which model explains the data better.

For comparison with the intracellular data, we performed an svd on the spike data for the same 15 cells that were used for the analysis of psps (Fig. 4A). One of these neurons fired a single spike in response to the 100-ms stimulus and behaved like a perfect digital AND gate in that 100% of the energy was in the first singular value. However, lower ranking singular values varied from neuron to neuron more widely in the spike data than in the membrane potential data. This variability caused the mean fractional energy for the first singular value to drop to 78.6 ± 40.7% (n = 15 neurons). Thus, the distribution of energy was more clearly biased toward the first singular value in the intracellular data than in the spike data. This departure from multiplication is partly due to additional nonlinear processes such as thresholding and nonlinear conversion of membrane potential to spikes (*7*) (Fig. 5). We also compared the multiplicative and additive models on the spike data. The reconstructed matrix fitted the data matrix better with multiplication than with addition (Fig. 4, B and C). The error of the fit was larger for the additive model than for the multiplicative one (F test, $P < 0.002$).

Examples of multiplication by neurons or neural circuits are scarce, although many computational models use this basic operation (*13*–*16*). Neurons of the monkey's posterior parietal lobe show "gain fields" that can be explained by a multiplication of retinal and eye or head position signals (*17*). The response of high-order visual neurons of locusts and pigeons predicts time of collision by multiplying the velocity of the retinal image edge with an exponential function of the size of the retinal image of the object (*18*, *19*). Behavior and high-order visual neurons in flies show responses that are consistent with coincidence detection, although the primary coincidence detectors remain to be identified (*20*). None of these studies identified the relevant psps that were multiplied, with one exception, in which postsynaptic inhibition was shown to underlie the directional sensitivity of the rabbit's visual ganglion cells (*21*). Mel and Koch (*22*) put forth a model in which multiplication of lower order receptive fields gives rise to a higher order receptive field. The owl's space-specific neurons behave like their model, although we do not know what biophysical mechanisms are involved. γ-Aminobutyric acid–mediated inhibition and *N*-methyl-D-aspartate–mediated responses in ICx might contribute to the multiplicative process (*23*, *24*).

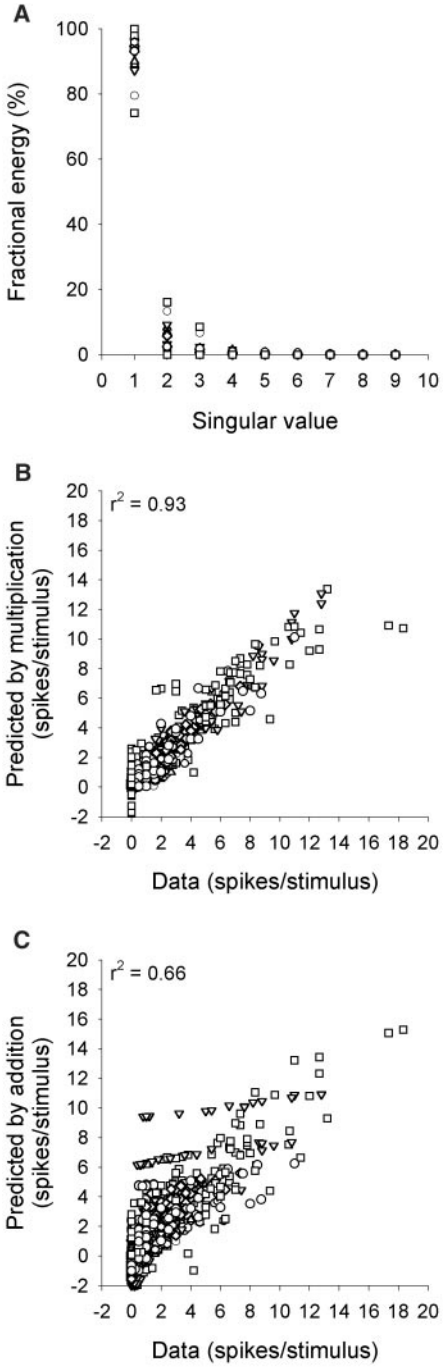

Fig. 4. Comparison of multiplicative and additive models for spikes data. (**A**) Fractional energy of singular values for spike data derived from the same set of neurons. Note shifts in fractional energy toward lower ranking singular values as compared with the membrane potential data (Fig. 3A). (**B**) Correlation between the number of spikes expected by multiplication and the data. Note a larger scatter here than in Fig. 3C. (**C**) The additive model fails to predict the spike data.

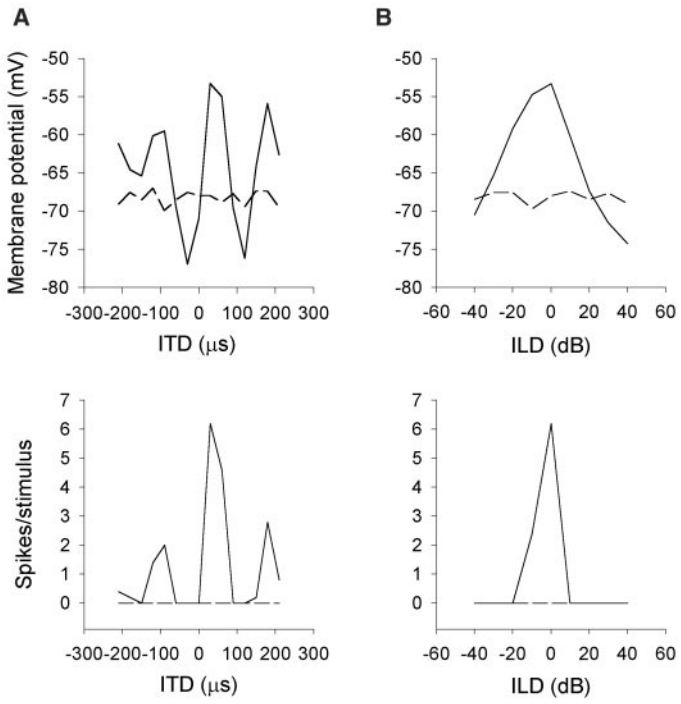

Fig. 5. Additional nonlinear processes in the formation of receptive fields. The translation from membrane potentials to spikes involves nonlinear processes other than multiplication. (**A**) ITD curve in mean membrane potentials (top) and ITD curve in mean spike rate per stimulus for the same neuron (bottom). (**B**) ILD curve in mean membrane potentials (top) and ILD curve in mean spike rate per stimulus for the same neuron (bottom). Resting membrane potential and spontaneous response are shown by dashed lines.

References and Notes

1. E. L. Knudsen, M. Konishi, *Science* **200**, 795 (1978).
2. A. Moiseff, M. Konishi, *J. Neurosci.* **3**, 2553 (1983).
3. W. E. Sullivan, M. Konishi, *J. Neurosci.* **4**, 1786 (1984).
4. T. T. Takahashi, A. Moiseff, M. Konishi, *J. Neurosci.* **4**, 1781 (1984).
5. Data were obtained from 14 adult barn owls (Tyto alba) of both sexes. Owls were anesthetized by initial intramuscular injections of ketamine hydrochloride (25 mg/kg; Ketaset, Fort Dodge) and diazepam (1.3 mg/kg; Western Medical Supply, Phoenix, AZ). Sharp glass electrodes filled with 2% neurobiotin in 2 M potassium acetate (pH 7.4) were advanced under visual control through a hole made on the bony cap containing the optic lobe. In all experiments, acoustic stimuli, broadband noise 100 ms in duration, 30 dB above threshold were delivered by an earphone assembly consisting of a Knowles ED-1914 receiver as a sound source, a Knowles BF-1743 damped coupling assembly for smoothing the frequency response of the receiver, and a calibrated Knowles 1939 microphone for monitoring sound pressure levels in the ear canal. Neural signals were amplified with an Axoclamp-2A intracellular amplifier, digitized, and stored by a computer at a sampling rate of 24 kHz. To visualize and measure synaptic potentials, we removed spikes using a median filter method (*6*). For more detailed methods, see (*7*).
6. B. Jagadeesh, H. S. Wheat, L. L. Kontsevich, C. W. Tyler, D. Ferster, *J. Neurophysiol.* **78**, 2772 (1997).
7. J. L. Peña, M. Konishi, *Proc. Natl. Acad. Sci. U.S.A.* **97**, 11787 (2000).
8. We could show that postsynaptic inhibitory potentials caused hyperpolarization, because we could reverse them by changing the membrane potential. However, because sound-evoked synaptic potentials often contained a mixture or balance of excitatory and inhibitory postsynaptic potentials, we refer to them as depolarizing and hyperpolarizing postsynaptic potentials, respectively.
9. E. I. Knudsen, M. Konishi, *Science* **202**, 778 (1978).
10. G. H. Golub, C. F. Van Loan, *Matrix Computations* (Johns Hopkins Univ. Press, Baltimore, MD, 1989).
11. Sound-induced mean spike rates or postsynaptic potentials plotted against ITD and ILD are referred to as ITD and ILD curves, respectively. To make an ITD or ILD curve, we kept one of the two inputs constant at its best value (referred to as best ILD and ITD). Space-specific neurons may respond to an ITD and ITD $\pm T$, where T is either the period of the stimulus tone or the inverse of the best frequency of the neuron (*7*).
12. The confidence limits are $\lambda \pm p_t\sigma/n^{1/2}$, where λ is the first singular values, p_t is a student random variable that varies with the confidence interval chosen and $n - 1$ degrees of freedom, σ is the standard deviation of the mean membrane potential, and n is the number of stimulus repetitions. The term $p_t\sigma/n^{1/2}$ represents the variability (noise) in the data.
13. T. Poggio, *Cold Spring Harbor Symp. Quant. Biol.* **55**, 944 (1990).
14. A. Pouget, T. J. Sejnowski, *J. Cognit. Neurosci.* **9**, 222 (1997).
15. E. Salinas, L. F. Abbott, *Proc. Natl. Acad. Sci. U.S.A.* **93**, 11956 (1996).
16. C. Koch, *Biophysics of Computation* (Oxford Univ. Press, Oxford, 1998).
17. R. A. Andersen, L. H. Snyder, D. C. Bradley, J. Xing, *Annu. Rev. Neurosci.* **20**, 303 (1997).
18. N. Hatsopoulos, F. Gabbiani, G. Laurent, *Science* **270**, 1000 (1995).
19. H. J. Sun, B. J. Frost, *Nature Neurosci.* **1**, 296 (1998).
20. M. Egelhaaf, A. Borst, W. Reichardt, *J. Opt. Soc. Am. A* **6**, 1070 (1989).
21. W. R. Taylor, S. He, W. R. Levick, D. I. Vaney, *Science* **289**, 2347 (2000).
22. B. W. Mel, C. Koch, in *Advances in Neural Information Processing Systems*, vol. 2, D. S. Touretzky, Ed. (Kaufmann, San Mateo, CA, 1990), pp. 474–481.
23. I. Fujita, M. Konishi, *J. Neurosci.* **11**, 722 (1991).
24. D. E. Feldman, E. I. Knudsen, *J. Neurosci.* **14**, 5939 (1994).

25. We thank P. Mitra and F. Gabbiani for their advice on using the svd, G. Kreiman and B. Christianson for their help with mathematics, C. Koch and G. Laurent for their enthusiasm and criticisms, C. Malek for computer matters, and G. Akutagawa for histology. This work was supported by NIH grant DC00134.

22 January 2001; accepted 9 March 2001

Josephson Junctions with Tunable Weak Links

Jan Hendrik Schön,[1]* Christian Kloc,[1] Harold Y. Hwang,[1] Bertram Batlogg[1,2]

The electrical properties of organic molecular crystals, such as polyacenes or C_{60}, can be tuned from insulating to superconducting by application of an electric field. By structuring the gate electrode of such a field-effect switch, the charge carrier density, and therefore also the superfluid density, can be modulated. Hence, weak links that behave like Josephson junctions can be fabricated between two superconducting regions. The coupling between the superconducting regions can be tuned and controlled over a wide range by the applied gate bias. Such devices might be used in superconducting circuits, and they are a useful scientific tool to study superconducting material parameters, such as the superconducting gap, as a function of carrier concentration or transition temperature.

Superconductivity is a most intriguing macroscopic quantum state, known for almost a century (*1*), yet still of great intellectual challenge and attraction, even as new classes of materials and new pairing mechanisms and order parameter symmetries are discovered. A particular consequence of the macroscopic quantum state is the occurrence of the Josephson effect when two superconductors are weakly connected. This effect is at the heart of practical devices such as ultrasensitive magnetic field detectors. In these devices, a carefully crafted thin insulating layer typically provides the coupling between superconductors. The coupling strength is exponentially sensitive to the insulator thickness and is fixed once the junction has been fabricated. However, it would be desirable to have an adjustable link, both in single-junction devices or in circuits where many superconductors could be Josephson-coupled and decoupled in an externally controlled way, as might be needed in quantum computing. We describe a method to create Josephson junctions where the coupling strength between two superconductors can be varied over the full possible range simply through the variation of an external voltage. It is based on the idea of controlling the superconducting properties of materials by an applied electric field (*2*). Such modulation has been demonstrated in a variety of field-effect devices (*3*–*9*). The technique of gate-induced superconductivity was used to exploit the capability of creating a controlled spatial modulation of the superfluid density within the same material through a suitable modification of the gate potential profile. Hence, an external

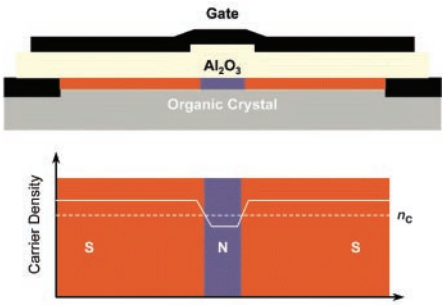

Fig. 1. Schematic of a "weak link" prepared on an organic single crystal. The cross-section of such a weak link shows the structured gate dielectric layer. By adjusting the gate voltage, a spatial variation of the carrier concentration can be achieved, which leads to the formation of a weak link [superconductor–normal conductor–superconductor (SNS) structure], although the details depend sensitively on the gate voltage, as seen in the insets of Fig. 3. Rather than forming a normal conducting region, a nonconducting (insulating) region appears to form.

[1]Bell Laboratories, Lucent Technologies, 600 Mountain Avenue, Murray Hill, NJ 07974–0636, USA. [2]Solid State Physics Laboratory, ETH Hönggerberg, CH-8093 Zürich, Switzerland.

*To whom correspondence should be addressed. E-mail: hendrik@lucent.com